Low-energy neutral atom signatures of magnetopause motion in response to southward B_z

Michael R. Collier, Thomas E. Moore, Mei-Ching Fok, Benjamin Pilkerton, and Scott Boardsen
NASA Goddard Space Flight Center, Greenbelt, Maryland, USA

Hina Khan
University of Leicester, Leicester, UK

Received 11 June 2004; revised 27 September 2004; accepted 29 October 2004; published 3 February 2005.

[1] We report an event observed by the Low-Energy Neutral Atom (LENA) imager on 18 April 2001, in which enhanced neutral atom emission was observed coming from the direction of the Sun and from the general direction of the subsolar magnetopause. The enhanced neutral atom emission is shown to be primarily a result of increased solar wind charge exchange with the Earth's hydrogen exosphere, that is, enhanced neutral solar wind formation, occurring in conjunction with a southward turning of the interplanetary magnetic field (IMF) which moves the magnetopause closer to the Earth. It is shown that the neutral atom flux under compressed magnetopause conditions is extremely sensitive to changes in the IMF north-south component.

Citation: Collier, M. R., T. E. Moore, M.-C. Fok, B. Pilkerton, S. Boardsen, and H. Khan (2005), Low-energy neutral atom signatures of magnetopause motion in response to southward B_z, *J. Geophys. Res.*, *110*, A02102, doi:10.1029/2004JA010626.

1. Introduction

[2] Although the solar atmosphere becomes fully ionized close to the Sun due to high coronal temperatures, with only about one neutral atom for every 10^7 protons, by the time the solar wind reaches the orbit of the Earth it contains a neutral component enhanced by many orders of magnitude [*Moore et al.*, 2003]. A variety of processes contribute to the enhanced neutral component including interactions with interplanetary and possibly interstellar dust, recombination, and charge exchange with neutral gas between the Sun and the Earth.

[3] The earliest references of which we are aware to the idea that the solar wind has a neutral component that may have observable consequences are *Dessler et al.* [1961], who considered it a potential source of background hydrogen atom flux for observations of proton ring current decay, and *Akasofu* [1964a, 1964b], who proposed that a neutral component of the solar plasma may be associated with geomagnetic storms (see also *Akasofu* [2002] for an historical account of the context of this proposal). The first experimental observations of the neutral component of the solar wind were reported by *Moore et al.* [2001], who analyzed the brightening of a "Sun signal" in neutral atom data in response to the Earth passage of a coronal mass ejection, and *Collier et al.* [2001a], who argued that the neutral solar wind signal was due to not only solar wind charge exchange with dust and interstellar neutrals but also was due to charge exchange with the Earth's hydrogen exosphere.

0148-0227/05/2004JA010626$09.00

[4] Further analysis of this neutral solar wind data showed that at various times and to various degrees this signal was due primarily to interplanetary dust [*Collier et al.*, 2003], interstellar neutrals or some other heliospheric source [*Collier et al.*, 2004], or charge exchange with the Earth's exosphere [*Collier et al.*, 2001b].

[5] In this latter study, *Collier et al.* [2001b] analyzed an event which occurred on 31 March 2001 and showed that during compressed time periods, magnetosheath neutral particle emission responds in a highly nonlinear manner to an increase in solar wind flux. This process is illustrated qualitatively by the two panels in Figure 1. The neutral flux, Φ_{NSW}, which is generated at the magnetopause and observed at a spacecraft such as IMAGE, will be proportional to the solar wind flux, Φ_{SW}, the geocoronal density at the magnetopause, n_{geo}, the effective line-of-sight, ℓ_{LOS}, and inversely proportional to the square of the distance to the source region, r. During periods of high solar wind flux, not only will the term Φ_{sw} increase but the magnetopause will be pushed closer to the Earth, resulting in higher values for n_{geo} and $1/r^2$. In addition, if the viewing is performed from above, as illustrated in Figure 1, the compressed magnetospheric condition will allow tangential viewing increasing the effective line of sight, ℓ_{LOS}. This is essentially limb brightening. A concise overview of these observations as well as of LENA neutral atom observations of ionospheric emissions may be found in the work of *Moore et al.* [2003].

[6] *Taguchi et al.* [2004a] have shown for an event on 11 April 2001 that an increase in solar wind ram pressure and a strong southward IMF moved the magnetopause inward, resulting in enhanced charge exchange with the

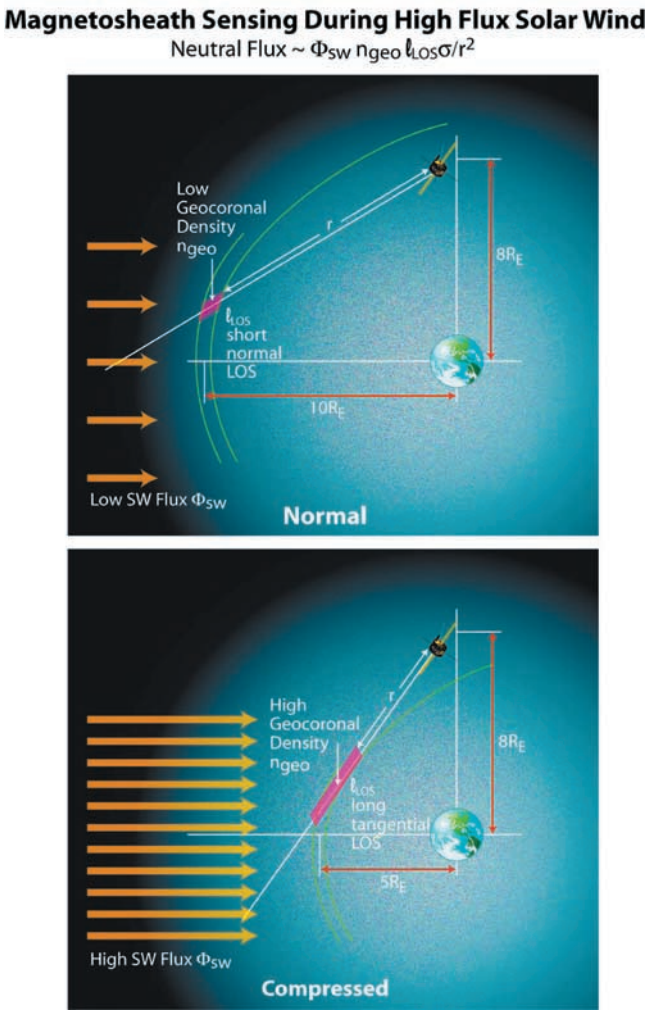

Figure 1. Magnetosheath neutral atom emission is greatly enhanced during periods of high flux solar wind due to the multiplicative effect of higher solar wind flux, Φ_{sw}, a more compressed magnetosphere which allows magnetosheath particles to sample higher exospheric densities, n_{geo}, tangential viewing allowing a longer effective line of sight, ℓ_{LOS}, and an emission region at distance r which moves closer to the spacecraft. The neutral flux is also proportional to the charge exchange cross section, σ.

Earth's hydrogen exosphere and increasing the flux of the postshocked neutral solar wind by a factor of three. They suggest that low-energy neutral atoms may be a means of monitoring cusp motion. In the study presented here, we can, to a large degree, separate the effect due to changes in the southward component of the IMF from changes in the solar wind ram pressure.

[7] The energetic neutral atom (ENA) emissions observed from the interaction of the solar wind with the Earth's magnetosphere have implications for other planets, as well. *Fok et al.* [2004] have shown that at Venus, because it has no intrinsic magnetic field, the solar wind penetrates deep into its upper atmosphere. Calculating neutral atom emissions using the global MHD model of *Tanaka and Murawski* [1997], Fok et al. show that energetic neutral atom emission from Venus' magnetosheath is comparable to or even greater than that of the Earth, leading to the natural conclusion that low-energy neutral atom imaging may be used to study the solar wind-Venus interaction, in particular loss rates which may be used to evaluate how Venus lost its water.

2. Overview of Observations on 18 April 2001

[8] Magnetosheath ENA emission increases dramatically when the magnetopause is pushed inward due to enhanced solar wind ram pressure. However, a southward turning of the interplanetary magnetic field (IMF), that is a negative B_z, even without a concomitant solar wind flux increase will move the magnetopause inward and effect increased ENA emission [*Yang et al.*, 2002; *Wiltberger et al.*, 2003]. Here we examine a time period when the solar wind flux was approximately constant and a southward turning of the IMF results in increased neutral atom emissions interpreted as due to the magnetopause moving closer to the Earth.

[9] Figure 2a shows the LENA background-corrected hydrogen data from the first 6 hours of 18 April 2001 (day 108). LENA responds to neutral hydrogen with energies from as low as 15 eV to at least 4 keV. The LENA data are presented in spectrogram format with time plotted on the x-axis and the spacecraft spin angle on the y-axis. The count rate of each of the 2 min by 8 degree pixels (summed over the 90 degree polar field of view) in this image is indicated logarithmically by the color whose range covers 2.5 orders of magnitude, as shown by the color bar on the right. The Sun signal representing neutral solar wind rides along the dashed line. The direction of the Earth is zero degrees azimuth with the Earth limb indicated by the two white lines.

[10] The level of activity in the spectrogram between the Sun and the Earth increases around 0050 UT. This increase in activity is associated with a sudden jump in solar wind density (based on time-shifted ACE observations) from about 5 cm^{-3} to 20–25 cm^{-3} and in solar wind speed from about 380 to 500 km/s. However, after 0100 UT, the solar wind flux remains very constant. The LENA data over the next 4 or so hours show that the peak emission occurs at about 0340, which corresponds to the maximum southward magnetic field observed at ACE traveling past the Earth. At the same time, a dramatic increase in the neutral solar wind flux coming from the direction of the Sun is observed.

[11] The bar at the top of the spectrogram indicates that the collimator which rejects charged particles was enabled until a bit after 0500 UT when enhanced fluxes of high-energy ions, whose presence is revealed by the relatively uniform (as a function of spin angle) high count rates, caused the collimator to automatically switch off.

[12] The three panels in the lower half of Figure 2 show the count rate distribution as a function of sector number (spacecraft spin angle) for three spins at various times during the periods shown in the spectrogram. These panels are cuts through the top spectrogram at the indicated times. The Earth direction, nadir, is approximately at sector 16, and in the first and third profiles

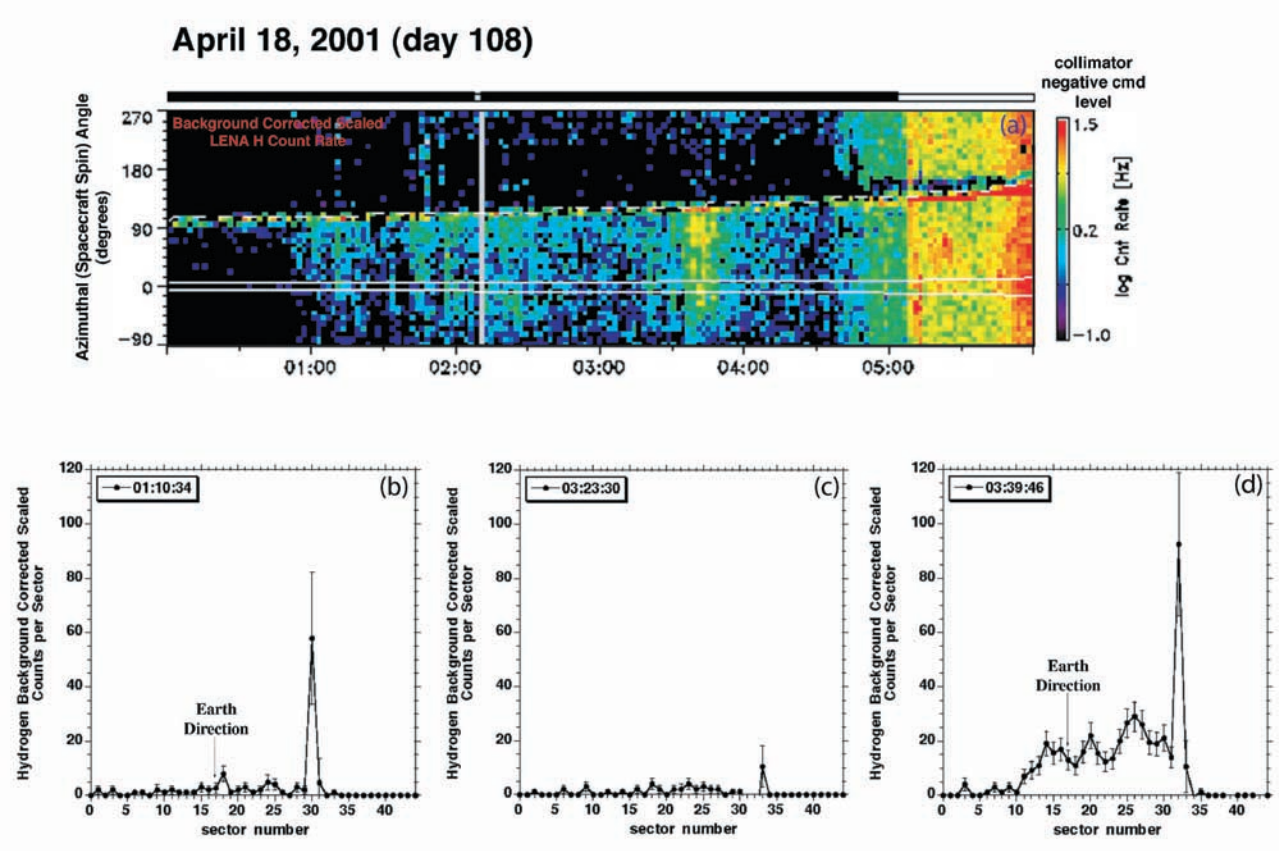

Figure 2. (a) A background-corrected hydrogen spectrogram covering all energies from the first 6 hours of 18 April 2001. The relatively uniform yellow color after about 0510 UT is characteristic of charged particle contamination and is a result of the collimator switching off (bar at top of panel). The two white lines near zero degrees indicate the angular extent of the Earth. (b)–(d) Count profiles as a function of sector number for three selected spins during this time period. The Earth center falls within sector 16. Note that there is modulation both in the Sun signal (falling in a sector between sector 30 and sector 33, depending on the panel) and in the diffuse emission observed primarily between the direction of the Earth and the direction of the Sun. The Sun signal is due primarily to solar wind protons charge exchanging prior to becoming slowed and heated by the bowshock. The diffuse emission is due to solar wind protons charge exchanging in the magnetosheath.

there is enhanced emission observed on the limb of the Earth. As is also apparent from these three panels, the Sun signal shows quite a bit of modulation, with a rough tendency to increase with the prominence of the signal between the Earth and the Sun. In comparison to the two earlier intervals, 0110:34 and 0323:30, the enhancement at 0339:46 also includes a brighter Sun signal near sector 32.

[13] Because this signal comes from within 8° or so of the direction of the Sun, it is attributable to charge exchange of the high Mach number solar wind prior to encountering the Earth's bow shock. The brightening of this narrow signal suggests the unshocked high Mach number solar wind is penetrating deeper into the Earth's exosphere before becoming heated and deflected by the bowshock. In other words, it indicates that the bowshock has moved closer to the Earth.

[14] Concomitant with the brightening of the Sun signal in the 0339:46 panel (Figure 2d), a diffuse emission appears mostly between the direction of the Sun and the Earth. This signal is interpreted as due to heated postshock solar wind charge exchanging with exospheric hydrogen between the bowshock and the magnetopause. During the time period between about 0100 and 0530 on 18 April 2001, Radio Plasma Imager (RPI) observations suggest that IMAGE was located in the magnetosheath (J. Green, private communication, 2004).

[15] This interpretation of the RPI observations appears reasonable based on an examination of the predictions of the *Roelof and Sibeck* [1993], *Shue et al.* [1997], and *Boardsen et al.* [2000] magnetopause models for where IMAGE is located relative to the magnetopause at various times during this event. All the models have IMAGE well inside the manetosphere prior to the event at 0030 UT while at 0130 UT, 0230 UT, and 0330 UT all models place IMAGE very close to the magnetopause and usually outside.

[16] It is not unusual to observe Sun signal brightening and magnetosheath signal in the LENA data in response to solar wind ram pressure increases which compress the

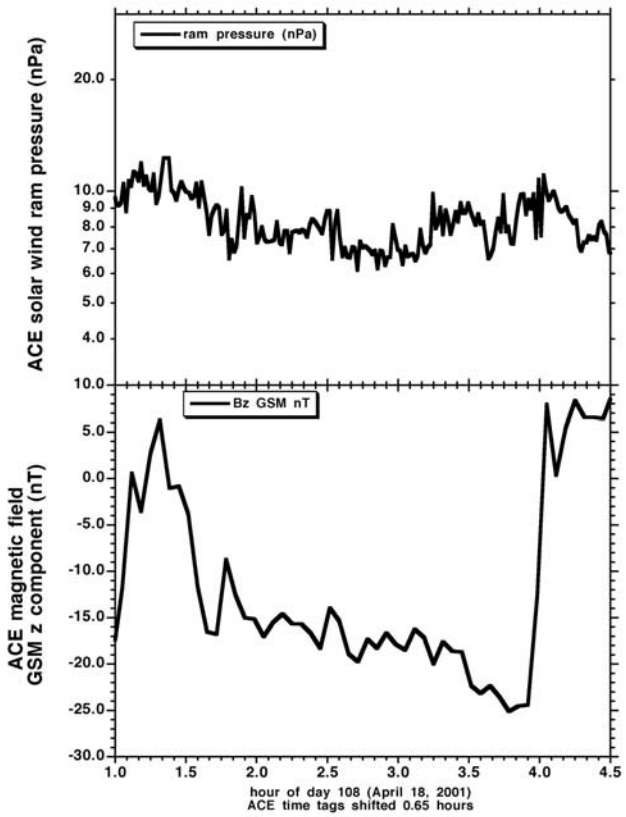

Figure 3. The top panel shows the solar wind ram pressure as measured by ACE upstream of the Earth, near L1, time shifted by 0.65 hours to account for the convection time from the spacecraft to the Earth. Note that the ram pressure remains constant over this time period, from about 0100–0430 to within about 25%. The lower panel shows the GSM z-component of the IMF measured at ACE again shifted by 0.65 hours. During the majority of the time interval, the field is strongly southward, reaching its peak southward excursion at about 0345 UT.

magnetosphere and allow the solar wind to access higher exospheric hydrogen densities which in turn results in higher rates of charge exchange [e.g., *Collier et al.*, 2001a, 2001b]. However, the top panel of Figure 3 shows the solar wind ram pressure in nPa, as measured by ACE over the time period LENA observes enhanced neutral atom emissions, 0100–0430 hours. The data are time-shifted 0.65 hours to account for the delay between observations at L1 and the IMAGE observations. The solar wind ram pressure was constant over this time period to within 25% or so, suggesting that it is unlikely that the enhanced and variable neutral atom fluxes, both the narrow emission from the direction of the Sun and the diffuse emission between the Earth and the Sun, are due to changes in solar wind ram pressure.

[17] However, the enhanced emission may very well be due to the magnetopause moving inward as a result of magnetopause erosion. The lower panel of Figure 3 shows the time-shifted ACE IMF GSM z-component over this same time period. The magnetic field is generally strong and southward, drifting (relatively steadily after 0145 UT) more negative from −5 to 10 nT down to about −25 nT in a few hour time period.

3. Quantitative Emission Model

[18] To test the idea that neutral atom emission from the magnetosheath is controlled, at least in part, by the southward component of the IMF, we present a simple magnetosheath neutral atom emission model to compare with the LENA observations. This model contains a number of idealizations which simplify considerably the calculations but still preserve the essential physics. The model is illustrated in Figure 4.

[19] Here, IMAGE is assumed located a distance r_{IM} above the Earth, where r_{IM} is taken to be 6 R_E. In actuality, IMAGE moves during the 5 hour period from about 2 to 4 R_E in front of the Earth and from about 8 to 4 R_E along the z-axis.

[20] The neutral atom emission is taken to originate from a small region of thickness l and characteristic size d near the nose of the magnetopause, which is at subsolar distance r_{mp}. This is also a simplification because one expects the characteristic length scales l and d to depend on other parameters such as subsolar magnetopause distance. Refer-

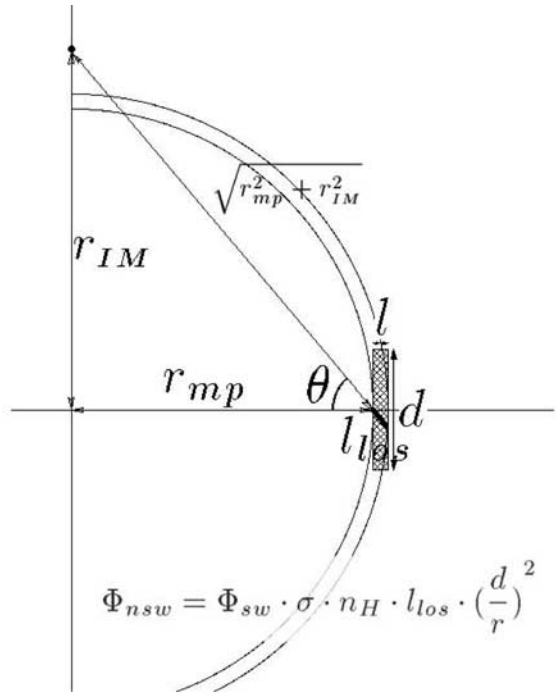

Figure 4. A simple analytic model for the neutral solar wind emission from near the magnetopause. The IMAGE spacecraft is taken to be along the z-axis a distance r_{IM} with the subsolar magnetopause position at r_{mp}. The source of the neutral solar wind emission is taken to be a region of width l and characteristic size d near the nose of the magnetopause. If the solar wind flux remains constant, the emission then depends on the product of the neutral density at the magnetopause nose, n_H, the line of sight, l_{los}, and one over the distance to the source region squared.

ring to Figure 4, the line of sight distance l_{los} through this region is given roughly by

$$l_{los} = l/\cos\theta = \frac{l\sqrt{r_{mp}^2 + r_{IM}^2}}{r_{mp}}, \quad (1)$$

where cos θ is the angle between the x-axis and the line connecting IMAGE to the nose of the magnetopause.

[21] The neutral atom flux from this region will drop off as approximately one over the distance from the source, r, squared or, referring to Figure 4, as

$$\left(\frac{d}{r}\right)^2 = \frac{d^2}{r_{mp}^2 + r_{IM}^2}. \quad (2)$$

[22] Finally, the local hydrogen exospheric density, n_H, falls off as approximately one over the distance from the Earth cubed [*Wallace et al.*, 1970; *Rairden et al.*, 1986] or as

$$n_H = n_{10R_E}\left(\frac{10R_E}{r_{mp}}\right)^3, \quad (3)$$

where n_{10R_E} is the exospheric density at 10 Earth radii, ~10 cm^{-3}. Note, however, exospheric neutral hydrogen densities are not spherically symmetric and exhibit time variability [*Østgaard et al.*, 2003].

[23] The neutral solar wind flux, Φ_{NSW}, due to charge exchange near the magnetopause nose that is observed by IMAGE is given by

$$\Phi_{NSW} = \Phi_{sw}\,\sigma n_H\, l_{los}\,(d/r)^2, \quad (4)$$

where Φ_{sw} is the solar wind flux and σ is the charge exchange cross section, about 2×10^{-15} cm^2. Using the above three expressions in equation (4),

$$\Phi_{NSW} = \Phi_{sw}\,\sigma n_{10R_E}(10R_E)^3 d^2\, l\, \frac{1}{{r_{mp}}^4}\, \frac{1}{\sqrt{r_{mp}^2 + r_{IM}^2}}. \quad (5)$$

[24] Note that expression (5) is extremely nonlinear in the magnetopause subsolar distance, r_{mp}. When $r_{IM} \gg r_{mp}$, the neutral solar wind flux varies as $1/r_{mp}^4$. When $r_{IM} \ll r_{mp}$, the neutral solar wind flux is even more sensitive, varying as $1/r_{mp}^5$. Of course, this model also does not take into account the magnetosheath flow lines which may favor polar viewing.

[25] It is also worth noting that global MHD models show a dayside structure for extreme southward IMF in which the reconnection region on the nose moves inward relative to the regions above and below. This creates a magnetopause surface which is more structured than that in Figure 4 with an inward dimple at the subsolar point [*Raeder et al.*, 2001].

[26] Interestingly, backscattered power from ground-based radar has been shown to be correlated with LENA sheath emissions [*Taguchi et al.*, 2004b]. For the event discussed here, the Tiger radar data show a strong correlation (~0.7) with the LENA observations with a time shift of 4 min [*Khan et al.*, 2003a]. Generally speaking, it is not surprising to find a correlation between the radar power and sheath emissions because both are affected by reconnection at the magnetopause. However, the interpretation of the Tiger radar data during this event appears to be more subtle.

[27] One possible interpretation is that the brightening in the LENA observations at about 0340 UT is partially related to the B_y component of the IMF shifting the reconnection area to produce more favorable viewing conditions for LENA [*Khan et al.*, 2003b; *McWilliams et al.*, 2001]. The IMF B_y component does affect the relative positions of the HF radar cusp which is approximately where the ionospheric footprint of the newly reconnected geomagnetic flux tubes is. Although this seems unlikely, a shift in the cusp location could have conceivably brought some active site into LENA's ±45 degree field of view.

4. Comparison With Observations

[28] In many magnetopause models, the dependence of the distance of the subsolar magnetopause, r_{mp}, from the Earth as the magnetic field varies at constant solar wind dynamic pressure is represented by a linear relationship with the z-component of the magnetic field, B_z:

$$r_{mp}(B_z) \propto \alpha + \beta \cdot B_z, \quad (6)$$

where α and β are constants and the expression is sometimes restricted only to southward B_z ($B_z < 0$) [e.g., *Petrinec and Russell*, 1996; *Chao et al.*, 2002; *Sibeck et al.*, 1991]. Although the qualitative results will not depend on the particular values of α and β used, for model purposes we will use the *Sibeck et al.* [1991] model

$$r_{mp}(B_z) = 11.3 + 0.25 \cdot B_z, \quad (7)$$

since there is no restriction on the sign of B_z. In expression (7), r_{mp} is in Earth radii while B_z is in nanotesla.

[29] On the other hand, the choice of the *Sibeck et al.* [1991] model can be criticized on a couple of grounds. First, it does not include the effects of the elevated ram pressure in the solar wind which places the magnetopause much closer than 11.3 R_E, without IMF effects. Second, the dependence on IMF B_z in this model is considerably larger than that of the other models considered by *Yang et al.* [2002].

[30] The left-hand axis and dashed line in Figure 5 show the magnetopause subsolar distance, r_{mp}, in Earth radii given the relationship in equation (7). Note that Figure 5 is not time-shifted. The right hand y-axis and solid line show the modeled magnetopause neutral solar wind flux, in arbitrary units, based on equation (5) and Figure 4. This figure shows graphically the behavior of equation (5), most notably that very small changes in the z-component of the magnetic field can effect very large changes in the neutral solar wind emission when the magnetopause is highly compressed.

[31] Indeed, extreme sensitivity to changes in B_z as small as 1 nT appears to be a general characteristic of magnetosheath emission. S. Taguchi et al. (Monitoring the high-latitude cusp with low-energy neutral atom imager: Simultaneous observations from IMAGE and Polar, in preparation for *Journal of Geophysical Research*, 2005) have observed this behavior for an event on 12 April 2001, as well.

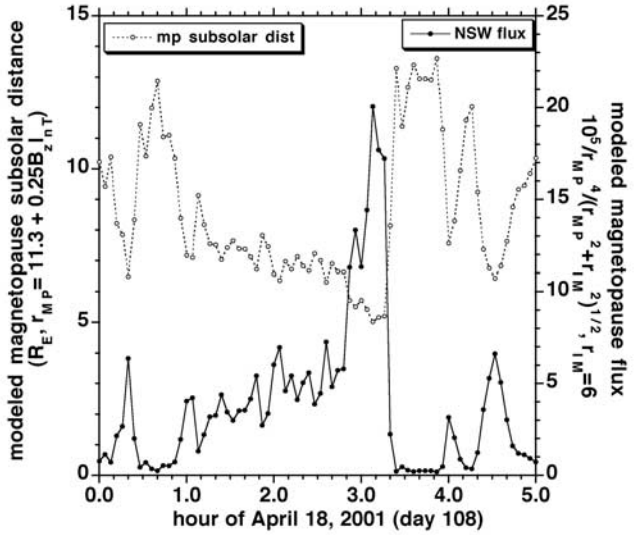

Figure 5. This figure shows both the predicted subsolar magnetopause location, based on the *Sibeck et al.* [1991] model (left hand y-axis and dashed line), and the modeled neutral solar wind flux based on the model shown in Figure 4 (right-hand y-axis and solid line). For the solid curve, IMAGE is taken to be at 6 R_E so that the modeled neutral solar wind flux depends only on the subsolar magnetopause distance. Note that this figure is not time-shifted.

[32] Figure 6 compares the observed LENA hydrogen emission from 0000 to 0500 hours on 18 April 2001 (day 108) between the Sun direction and the Earth direction (solid line and left-hand y-axis) with the (again unshifted for solar wind advection time) modeled emission from Figure 5 (dashed line and right-hand y-axis). In this figure, the observed LENA count rate falls over a seven sector range, about 56 degrees, between the direction of the Sun and the direction of the Earth. So, the rate does not include the direct Sun signal which rides along the white dashed line in the spectrogram in Figure 2, although this rate also generally correlates with the broader magnetosheath signal, as discussed in section 2. Even this relatively simple model results in good agreement with the observed neutral solar wind count rate.

[33] To further quantify this relationship, Figure 7 shows a time-shifted cross-correlation analysis between the model flux and the observed LENA flux. The peak correlation is 0.71 at a time shift of a bit over 32 min. For comparison, the solar wind convection time from ACE to 10 R_E is about 45 min. Depending on the relative orientation of the IMF phase fronts in the solar wind, the solar wind convection time may differ considerably from the true time difference between observations at different locations in the interplanetary medium [e.g., *Collier et al.*, 1998; *Weimer et al.*, 2002; *Crooker et al.*, 1982].

[34] Unfortunately, during this period, IMP-8 was very close to the nominal bow shock, Geotail was very close to the nominal magnetopause, and Wind was over 250 R_E off the Sun-Earth line, so it is not possible to get an accurate determination of the phase front orientation.

[35] A notable exception to the form given in equation (6) is the model of *Shue et al.* [1998] in which the effect of the

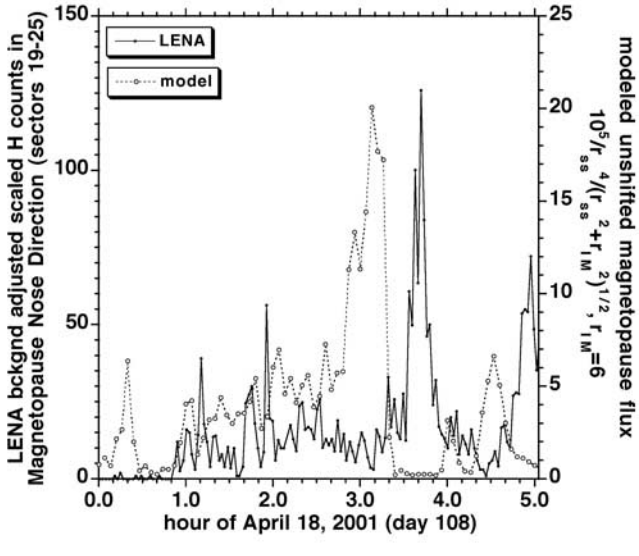

Figure 6. This figure compares the modeled neutral solar wind flux shown in Figure 5 (right-hand y-axis and dashed line) and the actual background adjusted scaled hydrogen atom counts observed in the general direction of the subsolar magnetopause, between the direction of the Sun and the Earth (sectors 19–25). Note that the modeled neutral solar wind flux is unshifted.

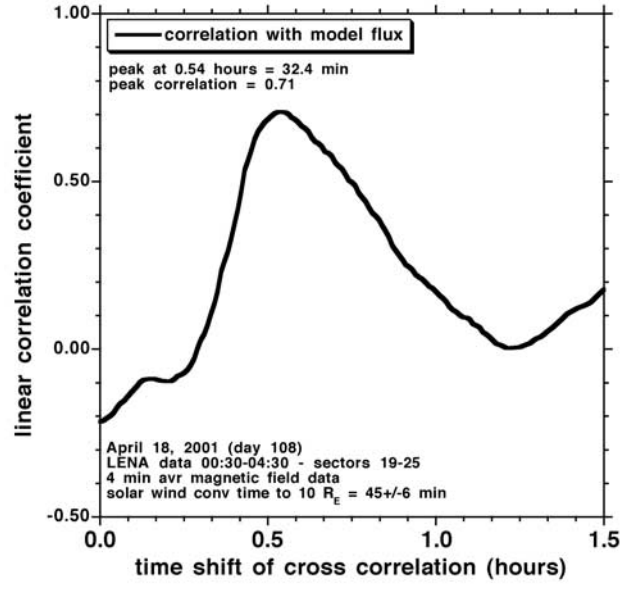

Figure 7. Results of a time lag cross correlation analysis between the LENA neutral hydrogen count rate in the magnetopause nose direction (sectors 19–25) and the analytic model predicted count rate. The peak correlation of 0.71 is at a time lag of a bit over 32 min, while the solar wind convection time is about 45 min.

interplanetary magnetic field B_z on the subsolar standoff distance saturates at large values. Because of the saturation effects, the Shue et al. model does reproduce the general increases and decreases observed in the LENA data, but without the structure predicted by the *Sibeck et al.* [1991] model. Consequently, an analysis similar to that described above produces a lag time profile similar to that shown in Figure 7 but with a much broader peak and lower amplitude.

5. Conclusions

[36] We have reported data from an event observed by the Low-Energy Neutral Atom (LENA) imager on 18 April 2001 in which enhanced neutral atom emission was detected coming from the direction of the Sun and from the general direction of the subsolar magnetopause. Because the solar wind ram pressure is approximately constant during this period, the enhanced neutral atom flux is interpreted to be primarily a result of increased solar wind charge exchange with the Earth's hydrogen exosphere due to the southward turning of the interplanetary magnetic field (IMF) which moved the magnetopause closer to the Earth.

[37] We presented a simple analytic model of magnetosheath neutral atom emission and compared the predictions of this model to the LENA data from 18 April 2001. The data correlate with the model predictions at the 0.71 level. One notable model prediction which appears substantiated by the LENA data is that neutral solar wind generation is highly sensitive to small changes in the southward component of the IMF when the magnetosphere is highly compressed.

[38] Understanding the magnetopause and magnetosheath boundaries, the coupling region between the solar wind and magnetosphere, will most likely require global imaging rather than sporadic in situ observations. With the diverse but complementary techniques of neutral atom imaging [*Collier et al.*, 2001a, 2001b], X-ray imaging [*Robertson and Cravens*, 2003], and radio plasma imaging [*Green and Reinisch*, 2003; *Nagano et al.*, 2003] which have been shown effective at remote sensing of the magnetopause and magnetosheath boundaries, the space physics community may be capable of producing, within reasonable resource constraints, a mission devoted to global magnetopause/magnetosheath remote sensing.

[39] **Acknowledgments.** ACE solar wind data were acquired via the ACE website. We thank the ACE SWEPAM and MAG instrument teams and the ACE Science Center for providing the ACE data. Special thanks to Mark Lester, Satoshi Taguchi, Stephen Fuselier, Harald Frey, and Gordon Wilson. Thanks also to the IMAGE Mission at GSFC for support.

[40] Shadia Rifai Habbal thanks Nikolai Østgaard and John G. Lyon for their assistance in evaluating this paper.

References

Akasofu, S.-I. (1964a), A source of the energy for geomagnetic storms and auroras, *Planet. Space Sci.*, *12*, 801–833.

Akasofu, S.-I. (1964b), The neutral hydrogen flux in the solar plasma flow - I, *Planet. Space Sci.*, *12*, 905–913.

Akasofu, S.-I. (2002), *Exploring the Secrets of the Aurora*, *Astrophys. Space Sci. Libr.*, vol. 278, pp. 21–25, Springer, New York.

Boardsen, S. A., T. E. Eastman, T. Sotirelis, and J. L. Green (2000), An empirical model of the high-latitude magnetopause, *J. Geophys. Res.*, *105*, 23,193–23,219.

Chao, J. K., D. J. Wu, C.-H. Lin, Y.-H. Wang, M. Kessel, S. H. Chen, and R. P. Lepping (2002), Models for the size and shape of the Earth's magnetopause and bow shock, in *Space Weather Study Using Multipoint Techniques*, *COSPAR Colloq. Ser.*, edited by L.-H. Lyu, 127–135, Elsevier, New York.

Collier, M. R., J. A. Slavin, R. P. Lepping, A. Szabo, and K. Ogilvie (1998), Timing accuracy for the simple planar propagation of magnetic field structures in the solar wind, *Geophys. Res. Lett.*, *25*, 2509–2512.

Collier, M. R., et al. (2001a), Observations of neutral atoms from the solar wind, *J. Geophys. Res.*, *106*, 24,893–24,906.

Collier, M. R., et al. (2001b), LENA observations on March 31, 2001: Magnetosheath remote sensing, *Eos Trans. AGU*, *82*(47), Fall Meet. Suppl., Abstract SM41C-05.

Collier, M. R., T. E. Moore, K. Ogilvie, D. J. Chornay, J. Keller, S. Fuselier, J. Quinn, P. Wurz, M. Wüest, and K. C. Hsieh (2003), Dust in the wind: The dust geometric cross section at 1 AU based on neutral solar wind observations, in *Solar Wind 10*, edited by M. Velli et al., *AIP Conf. Proc.*, *679*, 790–793.

Collier, M. R., T. E. Moore, D. Simpson, A. Roberts, A. Szabo, S. Fuselier, P. Wurz, M. A. Lee, and B. T. Tsurutani (2004), An unexplained 10°–40° shift in the location of some diverse neutral atom data at 1 AU, *Adv. Space Res.*, *34*, 166–171.

Crooker, N. U., G. L. Siscoe, C. T. Russell, and E. J. Smith (1982), Factors controlling degree of correlation between ISEE-1 and ISEE-3 interplanetary magnetic field measurements, *J. Geophys. Res.*, *87*, 2224–2230.

Dessler, A. J., W. B. Hanson, and E. N. Parker (1961), Formation of the geomagnetic storm main-phase ring current, *J. Geophys. Res.*, *66*, 3631–3637.

Fok, M.-C., T. E. Moore, M. R. Collier, and T. Tanaka (2004), Neutral atom imaging of solar wind interaction with the Earth and Venus, *J. Geophys. Res.*, *109*, A01206, doi:10.1029/2003JA010094.

Green, J. L., and B. W. Reinisch (2003), An overview of results from RPI on IMAGE, *Space Sci. Rev.*, *109*, 183–210.

Khan, H., M. R. Collier, T. E. Moore, M. Lester, S. Taguchi, and K. Hosokawa (2003a), Magnetosheath neutral atom observations and the relationship with radar backscatter in the cusp: Combined observations from IMAGE LENA and SuperDARN, *Eos Trans. AGU*, *84*(46), Fall Meet. Suppl., Abstract SM12A-1199.

Khan, H., M. Lester, J. A. Davies, S. E. Milan, and P. E. Sandholt (2003b), Multi-instrument study of the dynamic cusp during dominant IMF B_y conditions, *Ann. Geophys.*, *21*, 693–708.

McWilliams, K. A., S. E. Milan, T. K. Yeoman, J. B. Sigwarth, L. A. Frank, and M. Brittnacher (2001), Interplanetary magnetic field B_y dependence of the relative position of the dayside ultraviolet auroral oval and the HF radar cusp, *J. Geophys. Res.*, *106*, 29,027–29,036.

Moore, T. E., et al. (2001), Low energy neutral atoms in the magnetosphere, *Geophys. Res. Lett.*, *28*, 1143–1146.

Moore, T. E., M. R. Collier, M.-C. Fok, S. A. Fuselier, H. Khan, W. Lennartsson, D. G. Simpson, G. R. Wilson, and M. O. Chandler (2003), Heliosphere-geosphere interactions using low energy neutral atom imaging, *Space Sci. Rev.*, *109*, 351–371.

Nagano, I., X.-Y. Wu, H. Takano, S. Yagitani, H. Matsumoto, K. Hashimoto, and Y. Kasaba (2003), Remote sensing the magnetosheath by spin modulation of the terrestrial continuum radiation, *J. Geophys. Res.*, *108*(A6), 1224, doi:10.1029/2002JA009691.

Østgaard, N., S. B. Mende, H. U. Frey, G. R. Gladstone, and H. Lauche (2003), Neutral hydrogen density profiles derived from geocoronal imaging, *J. Geophys. Res.*, *108*(A7), 1300, doi:10.1029/2002JA009749.

Petrinec, S. M., and C. T. Russell (1996), Near-earth magnetotail shape and size as determined from the magnetopause flaring angle, *J. Geophys. Res.*, *101*, 137–152.

Raeder, J., Y. L. Wang, T. J. Fuller-Rowell, and H. J. Singer (2001), Global simulation of magnetospheric space weather effects of the Bastille Day storm, *Solar Phys.*, *204*, 325–338.

Rairden, R. L., L. A. Frank, and J. D. Craven (1986), Geocoronal imaging with Dynamics Explorer, *J. Geophys. Res.*, *91*, 13,613–13,630.

Robertson, I. P., and T. E. Cravens (2003), X-ray emission from the terrestrial magnetosheath, *Geophys. Res. Lett.*, *30*(8), 1439, doi:10.1029/2002GL016740.

Roelof, E., and D. G. Sibeck (1993), Magnetopause shape as a bivariate function of interplanetary field B_z and solar wind dynamic pressure, *J. Geophys. Res.*, *98*, 21,421–21,450.

Shue, J.-H., J. K. Chao, H. C. Fu, C. T. Russell, P. Song, K. K. Khurana, and H. J. Singer (1997), A new functional form to study the solar wind control of the magnetopause size and shape, *J. Geophys. Res.*, *102*, 9497–9511.

Shue, J.-H., et al. (1998), Magnetopause location under extreme solar wind conditions, *J. Geophys. Res.*, *103*, 17,691–17,700.

Sibeck, D. G., R. E. Lopez, and E. C. Roelof (1991), Solar wind control of the magnetopause shape, location, and motion, *J. Geophys. Res.*, *96*, 5489–5495.

Taguchi, S., M. R. Collier, T. E. Moore, M.-C. Fok, and H. J. Singer (2004a), Response of neutral atom emissions in the low-latitude and

high-latitude magnetosheath direction to the magnetopause motion under extreme solar wind conditions, *J. Geophys. Res.*, *109*, A04208, doi:10.1029/2003JA010147.

Taguchi, S., K. Hosokawa, M. R. Collier, T. E. Moore, M.-C. Fok, A. S. Yukimatu, N. Sato, and R. A. Greenwald (2004b), Simultaneous observations of the cusp with IMAGE Low Energy Neutral Atom Imager and SuperDARN radar, *Adv. Polar Upper Atmos. Res.*, *18*, 53–64.

Tanaka, T., and K. Murawski (1997), Three-dimensional MHD simulation of the solar wind interaction with the ionosphere of Venus: Results of two-component reacting plasma simulation, *J. Geophys. Res.*, *102*, 19,805–19,821.

Wallace, L., C. A. Barth, J. B. Pearce, K. K. Kelly, D. E. Anderson Jr., and W. G. Fastie (1970), Mariner 5 measurement of the Earth's Lyman alpha emission, *J. Geophys. Res.*, *75*, 3769–3777.

Weimer, D. R., D. M. Ober, N. C. Maynard, W. J. Burke, M. R. Collier, D. J. McComas, N. F. Ness, and C. W. Smith (2002), Variable time delays in the propagation of the interplanetary magnetic field, *J. Geophys. Res.*, *107*(A8), 1210, doi:10.1029/2001JA009102.

Wiltberger, M., R. E. Lopez, and J. G. Lyon (2003), Magnetopause erosion: A global view from MHD simulation, *J. Geophys. Res.*, *108*(A6), 1235, doi:10.1029/2002JA009564.

Yang, Y.-H., J. K. Chao, C.-H. Lin, J.-H. Shue, X.-Y. Wang, P. Song, C. T. Russell, R. P. Lepping, and A. J. Lazarus (2002), Comparison of three manetopause prediction models under extreme solar wind conditions, *J. Geophys. Res.*, *107*(A1), 1008, doi:10.1029/2001JA000079.

S. Boardsen, M. R. Collier, M.-C. Fok, T. E. Moore, and B. Pilkerton, Laboratory for Extraterrestrial Physics, NASA Goddard Space Flight Center, Greenbelt, MD 20771, USA. (michael.r.collier@nasa.gov)

H. Khan, European Space Research and Technology Centre, Keplerlaan 1, Postbus 299, 2200 AG Noordwijk ZH, Netherlands.